

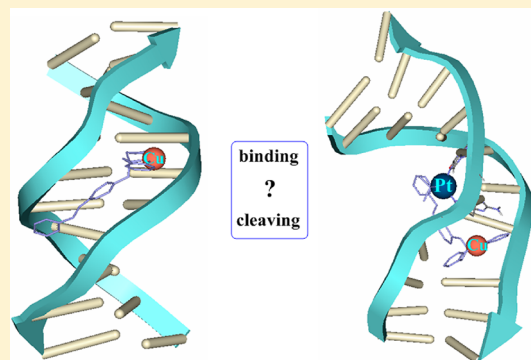
Theoretical Simulations on Interactions of Mono- and Dinuclear Metallonucleases with DNA

Chunmei Liu, Yanyan Zhu,* Peipei Chen, and Mingsheng Tang*

The College of Chemistry and Molecular Engineering, Zhengzhou University, Zhengzhou, Henan Province 450001, PR China

 Supporting Information

ABSTRACT: In the present study, molecular dynamic simulations have been performed to investigate the DNA binding affinities and cleavage activities of a new class of mononuclear copper (*p*-Cu(BPA) and *m*-Cu(BPA)) and dinuclear copper–platinum (*p*-Cu(BPA)-Pt and *m*-Cu(BPA)-Pt) metallonucleases. The simulated results reveal that the two mononuclear nucleases are noncovalent minor groove DNA binders and the two dinuclear ones tend to be bound to DNA in the major groove by a covalent bond between the platinum center and N7 of the guanine base, which is in agreement with the experimental results. The simulated results show that the binding affinities of the four studied nucleases with DNA are in the order of *p*-Cu(BPA) < *m*-Cu(BPA) < *p*-Cu(BPA)-Pt < *m*-Cu(BPA)-Pt; the binding affinities are dominated by intermolecular binding modes of nucleases with DNA and the intermolecular hydrogen bonds. The distance probability distributions indicate that the hydrogen atoms of DNA sugar could be abstracted by the four nucleases. Specifically, the dinuclear nucleases abstract hydrogen atoms from the deoxyribose sugar linking to G₁₈ base while mononuclear nuclease abstracts hydrogen atoms from the deoxyribose sugars linking to C₁₅ and C₁₆ bases, suggesting that the dinuclear nucleases improve the sequence-selective cleavage of DNA compared with the mononuclear one. Moreover, the differences in calculated DNA conformational dynamics and groove parameters demonstrate that the extent of DNA conformational distortions induced by dinuclear nucleases is greater than that induced by mononuclear nucleases. This investigation provides detailed information showing that dinuclear nucleases have superior DNA binding affinities and nuclease activities as compared with their mononuclear counterparts.



1. INTRODUCTION

Artificial metallonucleases have received tremendous interest for their diverse potentials in biotechnology and in medicine. They are promising candidates for application in cancer therapy as well.^{1–3} In the presence of reactive oxygen species, metallonucleases could attack the sugar or base moieties of DNA, then achieve strand scission of DNA, which leads to disruption of the transcription and/or replication, initiating ultimately the death and mutagenesis of cancer cells.⁴ Particularly, transition metal complexes stand out as candidates for artificial metallonucleases due to their structural and functional varieties.^{5,6} A large number of transition metal complexes of Fe, Cu, Ni, Pt, Ru, Rh, and Mn have been validated to damage DNA efficiently in a relevant environment.^{7–13} In recent years, the exploration of copper complexes as chemical nucleases has seen an upsurge because they possess biologically accessible redox potentials and high nucleobase affinities.^{14–16} Actually, there has been an increasing interest in DNA binding and cleavage properties of mixed ligand copper complexes and in designing a great deal of new copper-based metallodrugs.^{17–21}

However, it is still a challenge for most copper nucleases to cleave DNA with high nucleic acid sequence specificity.^{22,23} Many experimental and theoretical strategies were proposed to

achieve the selective cleavage of certain DNA sequences by copper nucleases.^{24,25} Specifically, DNA-specific recognition agents²⁵ and multinuclear complexes^{26,27} were developed to achieve targeted strand scission. For example, the introduction of recognition agents could improve the selectivity of DNA cleavage of copper-based nucleases in the previous work.²⁸ Pitié and co-workers have found that copper complexes including Clip-Phen ligand or derivatives exhibit a dramatic increase of the DNA cleavage activity and perform highly selective cleavage at successional sequences of DNA assisted by nucleic acids sequence recognition agents.^{14,16,25,28–34} Multinuclear metal centers are found to display synergistic effects in the selective cleavage of DNA.^{26,27} Especially, multinuclear copper complexes offer the possibilities for specific DNA binding and cleavage.^{35,36} Karlin and co-workers have reported a series of dinuclear and trinuclear copper complexes with flexible linkers that presented promising DNA-cleaving specificity.^{37,38} Moreover, Reedijk and co-workers have synthesized dinuclear compounds of platinated copper(3-Clip-Phen) which exhibited higher DNA cleavage efficiency and specificity. Their study

Received: July 15, 2012

Revised: January 9, 2013

Published: January 14, 2013

Chart 1. Structures of Two Mononuclear Copper Nucleases and Two Dinuclear Copper–Platinum Nucleases: (a) *p*-Cu(BPA), (b) *m*-Cu(BPA), (c) *p*-Cu(BPA)-Pt, and (d) *m*-Cu(BPA)-Pt

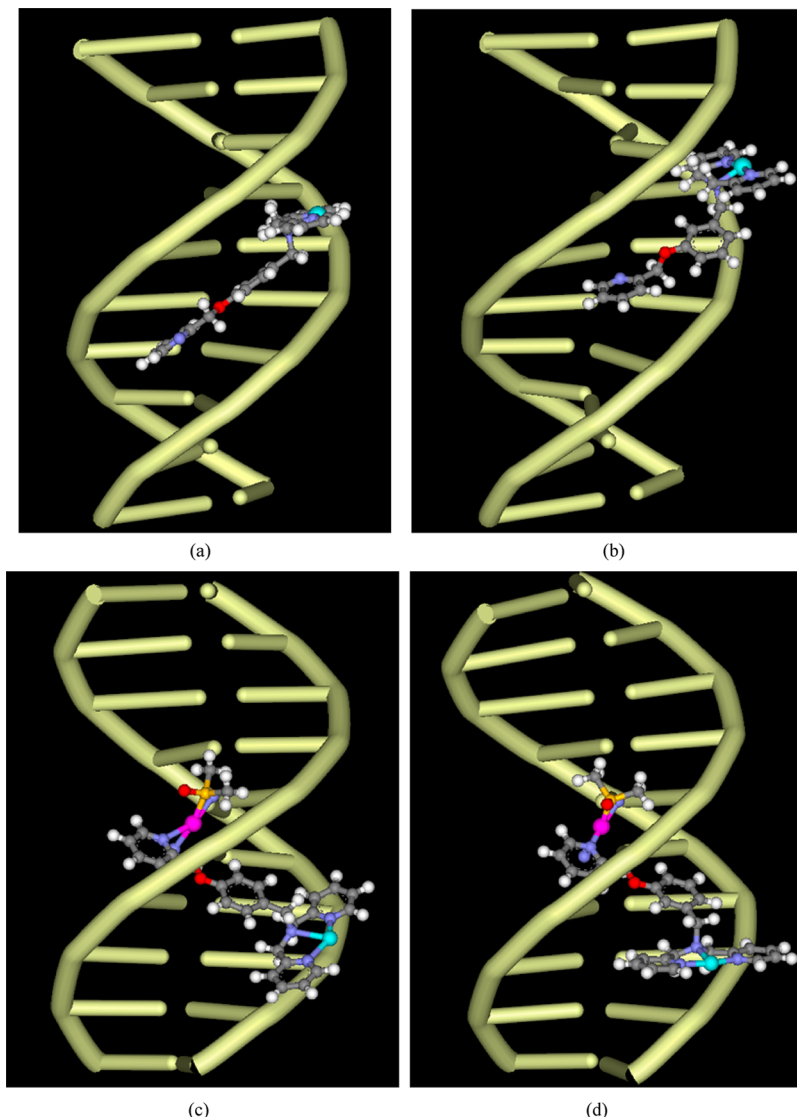
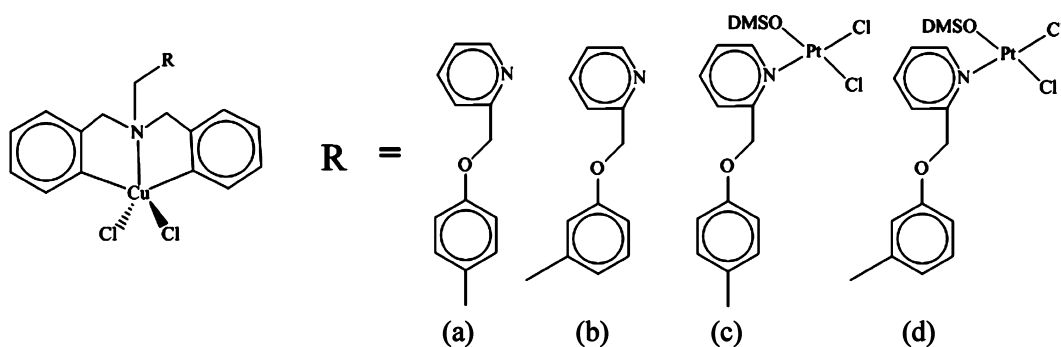


Figure 1. Binding modes of mononuclear copper nucleases *p*-Cu(BPA)/*m*-Cu(BPA) and dinuclear copper–platinum nucleases *p*-Cu(BPA)-Pt/*m*-Cu(BPA)-Pt with DNA: (a) *p*-Cu(BPA)-DNA, (b) *m*-Cu(BPA)-DNA, (c) *p*-Cu(BPA)-Pt-DNA, and (d) *m*-Cu(BPA)-Pt-DNA (copper in cyan, platinum in magenta, carbon in gray, nitrogen in blue, oxygen in red, and hydrogen in white).

suggested that the platinum component might act as a DNA anchor inducing DNA strand scission in a sequence-selective fashion.^{39–41}

Encouraged by the successful antitumor activities of these complexes, Guo's group have synthesized four copper

nucleases⁴² as presented in Chart 1 (*p*-Cu(BPA) and *m*-Cu(BPA) are mononuclear copper nucleases, *p*-Cu(BPA)-Pt and *m*-Cu(BPA)-Pt are dinuclear copper–platinum nucleases). Their experimental results demonstrated that the binding affinities and cleavage abilities of dinuclear copper–platinum

nucleases are stronger than those of the corresponding mononuclear copper nucleases. Especially, the dinuclear copper–platinum nucleases exhibit site-specific cleavage of DNA. However, the reasons for the better DNA binding affinity, cleavage activity, and site-selectivity of dinuclear copper–platinum nucleases are not clear because of the lack of structural studies. Molecular dynamics (MD) simulations provide a powerful tool for studying the structures and interaction potentials for the biological macromolecules with analogized biological environment.^{43–49}

In this work, we used molecular dynamics simulations to investigate the binding affinities and cleavage abilities of the four nucleases shown in Chart 1. We started the work by studying the interactions between mononuclear/dinuclear nucleases and DNA decamer d(5'-CTCTGGTCTC-3')₂, the sequence used in Guo's experimental studies.⁴² We then examined the differences in DNA conformational dynamics of these nuclease–DNA adducts. A series of five independent MD simulations have been carried out, the first two MD simulations were performed on adducts of the two mononuclear copper nucleases, *p*-Cu(BPA) and *m*-Cu(BPA), with DNA to study their binding affinity and cleavage ability; the second two simulations were performed on adducts of two dinuclear copper–platinum nucleases, *p*-Cu(BPA)-Pt and *m*-Cu(BPA)-Pt, with DNA to address the dinuclear nucleases have superior DNA binding ability and cleavage efficiency as compared with their mononuclear counterparts, and the platinum centers of dinuclear nucleases play a site-cleavage role in DNA strand scission; the last one was performed on the standard B-DNA molecule to study the conformational dynamics differences between the damaged DNA included in adducts and the undamaged DNA.

2. MODELS AND COMPUTATIONAL METHODS

2.1. Initial Structures. The initial structures of the four nucleases were optimized by using the Gaussian 09 program.⁵⁰ Geometry optimizations were carried out by using the hybrid B3LYP^{51,52} functional together with the 6-31G(d, p) basis set for C, H, O, Cl, and N atoms, DZpdf⁵³ basis set for the Cu atom, and Lanl2dz^{54,55} basis set for the Pt atom. The initial B-DNA structure of d(5'-C₁T₂C₃T₄G₅G₆T₇C₈T₉C₁₀-3')-d(5'-G₁₁A₁₂G₁₃A₁₄C₁₅C₁₆A₁₇G₁₈A₁₉G₂₀-3'), which was not obtained as a crystal structure in the experiment,⁴² was generated by using the *nucgen* module of the AMBER11 package.^{56,57} The Autodock4.0 program⁵⁸ was employed to evaluate the binding modes between *p*-Cu(BPA)/*m*-Cu(BPA) and DNA with use of the Lamarckian genetic algorithm (LGA).⁵⁸ The scoring function of the empirical free energies for the docked configurations has been tested for all docking models. The grid consisted of 88 × 106 × 86 points with a grid spacing of 0.375 Å. From the 1000 docking prediction modes estimated by the docking process for each nuclease with DNA, we chose the better-scoring representative conformations as an initial structure (assigned as *p*-Cu(BPA)-DNA and *m*-Cu(BPA)-DNA, as shown in parts a and b of Figure 1) for MD simulations. To generate starting structures for dinuclear nucleases with DNA adducts, two N7 atoms of the adjacent guanine bases (G₅G₆) were bound to the platinum atom, the Cu moiety toward the minor groove of DNA⁴² (assigned as *p*-Cu(BPA)-Pt-DNA and *m*-Cu(BPA)-Pt-DNA, as shown in Figure 1c,d). Given that each strand of DNA has phosphate groups, Na⁺ counterions were added to the corresponding system to achieve electroneutrality. The systems were explicitly

solvated by using the TIP3P water potential inside a box large enough to ensure the solvent shell extended to 10 Å in all directions of each studied system. Periodic boundary conditions were used in all three directions. All the simulations with slightly different poses for each simulated system have converged to one structure after the corresponding courses of simulations. Therefore, all structures referred to in this work are these converged ones.

2.2. Force Field Parameters. The atom types for the studied four nucleases, except for the copper and platinum atoms, were generated by using the ANTECHAMBER module in the AMBER11 program⁵⁷ (shown in Figure S1 in the Supporting Information). The electrostatic potentials of the four different nucleases used for RESP charge calculations were obtained by calculating the optimized structures at the HF/6-31G(d)⁵⁹ level with the Gaussian09 program.⁵⁰ The RESP charges of these nucleases were then derived by the RESP program based on the calculated electrostatic potentials. Specifically, the RESP charges of the copper atom in *p*-Cu(BPA), *m*-Cu(BPA), *p*-Cu(BPA)-Pt, and *m*-Cu(BPA)-Pt are 0.981, 1.024, 0.241, and 0.357 and those of the platinum atom in *p*-Cu(BPA)-Pt and *m*-Cu(BPA)-Pt are 0.667 and 0.581, respectively, as shown in Table 1. The force field parameters of

Table 1. RESP Charges of the Four Studied Nucleases

atom type	<i>p</i> -Cu(BPA)	<i>m</i> -Cu(BPA)	<i>p</i> -Cu(BPA)-Pt	<i>m</i> -Cu(BPA)-Pt
CA	-0.042	-0.040	-0.074	-0.102
C3	-0.279	-0.179	-0.097	-0.081
NB	-0.235	-0.257	0.183	0.105
N3	-0.046	-0.159	-0.052	-0.091
OS	-0.025	0.028	-0.062	-0.165
HA	0.126	0.118	0.138	0.157
H1	0.185	0.164	0.111	0.109
S			0.164	0.166
Cu	0.981	1.024	0.241	0.357
Pt			0.667	0.581

the copper center and platinum center of the studied nucleases, including the vdW parameters and bonded parameters, were adopted from previous works.^{28,47,60,61} Other force field parameters of the nucleases were generated from the gaff force field in the AMBER11 program.⁵⁷

2.3. MD Simulations. All simulations were carried out by using the SANDER module of the AMBER11 program package⁵⁷ with the parm99⁶² force field of AMBER together with the parmbsc0⁶⁰ refinement and gaff⁶³ force field parameters. The protocol for all MD simulations is described in detail in the Supporting Information. Each system was simulated for 40 ns and 40 000 structures for each simulation were saved for postprocessing by uniformly sampling the trajectory.

2.4. DNA Helical Parameters Analysis. To address the effect of nuclease on DNA conformational dynamics, the frequency distributions of DNA helical parameters at the base pair of DNA near the binding sites along with the canonical B-DNA molecule were analyzed for statistical significance by the Kolmogorov–Smirnov test. The Kolmogorov–Smirnov test determines how significantly these distributions differ from each other without making any assumptions regarding the distribution of data (nonparametric and distribution-free).⁴⁷ The calculations of all DNA helical parameters were carried out with the CURVES program.⁶⁴ Specifically, the PTraj module

of the AMBER11 program was used to extract production conformations. These extracted snapshots were saved in Protein Data Bank (PDB) format. Each nucleotide type was converted from the AMBER format to PDB format, and the resulting snapshots were submitted to the CURVES program.⁶⁴ The following DNA helical parameters were extracted—base pair helical parameters: shear, buckle, and propeller; and base pair step helical parameters: shift, roll, and twist. Percentage occupancy distributions of the DNA helical parameters were calculated by normalizing the frequency distributions to 100%. These helical parameters can be used to measure the extent of a DNA structure deviation from its canonical B-DNA.⁶⁵

2.5. MM_PBSA Approach. The MM_PBSA method has proven useful to investigate drug molecules binding in the minor groove of DNA in the study of a variety of nucleic acid systems.^{66,67} Energetic postprocesses for each MM_PBSA calculation were carried out by using MM_PBSA module of the AMBER11 program through molecular mechanics and a continuum solvent model. Binding free energy, $\Delta G_{\text{binding}}$, is estimated by the free energy difference between nuclease, DNA, and adduct. Specifically, binding free energy ($\Delta G_{\text{binding}}$) for nuclease and DNA was estimated by:

$$\Delta G_{\text{binding}} = G_{\text{adduct}} - G_{\text{DNA}} - G_{\text{nuclease}}$$

where G_{adduct} , G_{DNA} , and G_{nuclease} are the free energies of adduct, DNA, and nuclease molecules, respectively.⁶⁸ The free energy (G) of each state is estimated from molecular mechanical energy E_{MM} , solvation free energy G_{SOLV} , and solute entropy S , respectively.

$$G = E_{\text{MM}} + G_{\text{SOLV}} - TS$$

$$E_{\text{MM}} = E_{\text{int}} + E_{\text{vdw}} + E_{\text{ele}}$$

$$G_{\text{SOLV}} = G_{\text{pb/solv}} + G_{\text{np/solv}}$$

where T is temperature, E_{int} is internal energy, E_{vdw} is the average van de Waals energy, E_{ele} is the average electrostatic energy, and $G_{\text{pb/solv}}$ is the polar solvation free energy computed from the finite difference Poisson–Boltzmann method in the DelPhi program of AMBER11. The dielectric constants inside and outside the molecule were 1.0 and 80.0, respectively; $G_{\text{np/solv}}$ is nonpolar solvation free energy, which was determined from the equation as follows:

$$G_{\text{np/solv}} = \gamma \text{SASA} + b$$

where SASA is the solvent accessible surface area, and is estimated by using Sanner's algorithm implemented in the Molsurf module included in AMBER11 with a probe radius of 1.4 Å; γ and b are the surface tension proportionality constant of 0.00542 kcal·mol⁻¹·Å⁻² and the free energy of nonpolar solvation for a point solute of 0.92 kcal·mol⁻¹, respectively. Additionally, the solute entropy, S , was estimated by normal mode calculations by using the NMODE module included in AMBER11.

3. RESULTS AND DISCUSSION

It is considered that flat trend of root-mean-square deviation (RMSD) fluctuation indicates a stable state of the system.⁶⁹ The trend of the RMSD values for the whole structure of each studied system referenced to the corresponding starting structures presents flat during the course of each 40 ns simulation, indicating that the current simulation protocol is

sufficiently accurate to describe these kinds of adduct systems (shown in Figure S2 in the Supporting Information).

3.1. Binding Affinity of Four Nucleases. On the basis of obtained experimental results,^{42,70,71} it is obviously found that the nucleases *p*-Cu(BPA)-Pt/*m*-Cu(BPA)-Pt are bound to DNA through covalent bonds of the platinum atom with N7 of guanines while the nucleases *p*-Cu(BPA)/*m*-Cu(BPA) are noncovalent DNA minor groove binders. The platinum center plays an important role in covalent binding interaction between dinuclear nucleases *p*-Cu(BPA)-Pt/*m*-Cu(BPA)-Pt and DNA. The covalent interaction between two molecules is known to be much stronger than that of noncovalent interaction. Therefore, the DNA binding affinities of *p*-Cu(BPA)-Pt/*m*-Cu(BPA)-Pt are higher than those of *p*-Cu(BPA)/*m*-Cu(BPA). The apparent DNA binding constants (K_{app}) of the four nucleases *p*-Cu(BPA), *m*-Cu(BPA), *p*-Cu(BPA)-Pt, and *m*-Cu(BPA)-Pt determined in Guo's experiment were 1.16×10^5 , 1.34×10^5 , 1.47×10^5 , and 3.42×10^5 M⁻¹, respectively.⁴² The binding affinities of the four nucleases are in the order of *p*-Cu(BPA) < *m*-Cu(BPA) < *p*-Cu(BPA)-Pt < *m*-Cu(BPA)-Pt.

To investigate the different binding affinities of *p*-Cu(BPA) and *m*-Cu(BPA), binding free energies of *p*-Cu(BPA)/*m*-Cu(BPA) with DNA were estimated by the MM_PBSA approach;^{66,72} the calculated MM-PBSA energies can provide the interaction details for the binding affinities of nucleases with DNA. Table 2 shows all energy terms and the total binding free

Table 2. Binding Free Energy Components (kcal·mol⁻¹) for Adducts of *p*-Cu(BPA)-DNA and *m*-Cu(BPA)-DNA^a

	<i>p</i> -Cu(BPA)-DNA	<i>m</i> -Cu(BPA)-DNA
ΔE_{ele}	-459.5	-425.0
ΔE_{vdw}	-43.8	-40.9
ΔE_{int}	-0.0	-0.0
ΔE_{MM}	-503.3	-466.0
$\Delta G_{\text{np/solv}}$	-5.0	-4.9
$\Delta G_{\text{pb/solv}}$	476.4	437.3
ΔG_{SOLV}	471.4	432.4
ΔG_{pb}	16.9	12.3
ΔG_{np}	-48.8	-45.8
$\Delta E_{\text{MM}} + \Delta G_{\text{SOLV}}$	-31.9	-33.6
$T\Delta S$	-24.0	-22.3
$\Delta G_{\text{binding}}$	-7.9	-11.3

^aVan de Waals energy: ΔE_{vdw} ; electrostatics energy: ΔE_{ele} ; nonpolar solvation free energy: $\Delta G_{\text{np/solv}}$; polar solvation free energy: $\Delta G_{\text{pb/solv}}$; solvation free energy ($\Delta G_{\text{SOLV}} = \Delta G_{\text{np/solv}} + \Delta G_{\text{pb/solv}}$); total nonpolar energy: $\Delta G_{\text{np}} = \Delta E_{\text{vdw}} + \Delta G_{\text{np/solv}}$; total polar energy: $\Delta G_{\text{pb}} = \Delta E_{\text{ele}} + \Delta G_{\text{pb/solv}}$; binding free energy: $\Delta G_{\text{binding}} = \Delta E_{\text{MM}} + \Delta G_{\text{SOLV}} - T\Delta S = \Delta E_{\text{ele}} + \Delta E_{\text{vdw}} + \Delta E_{\text{int}} + \Delta G_{\text{np/solv}} + \Delta G_{\text{pb/solv}} - T\Delta S = (\Delta E_{\text{ele}} + \Delta G_{\text{pb/solv}}) + (\Delta E_{\text{vdw}} + \Delta G_{\text{np/solv}}) - T\Delta S = \Delta G_{\text{pb}} + \Delta G_{\text{np}} - T\Delta S$; ($\Delta E_{\text{int}} = 0$).

energies. As expected, the calculated binding free energy of *m*-Cu(BPA) with DNA ($\Delta G_{\text{binding}} = -11.3$ kcal·mol⁻¹) is lower than that of *p*-Cu(BPA) with DNA ($\Delta G_{\text{binding}} = -7.9$ kcal·mol⁻¹). Hence, *m*-Cu(BPA) has a higher binding affinity with DNA compared with *p*-Cu(BPA), which agrees fairly well with the experimental results.⁴² As shown in Table 2, the intermolecular vdW interaction (ΔE_{vdw}) and the nonpolar contribution to solvation ($\Delta G_{\text{np/solv}}$) provide the driving force for binding. The total nonpolar energies ($\Delta G_{\text{np}} = \Delta E_{\text{vdw}} + \Delta G_{\text{np/solv}}$ -48.8 and -45.8 kcal·mol⁻¹ for *p*-Cu(BPA) and *m*-Cu(BPA), respectively) are favorable for the formation of both *p*-Cu(BPA)-DNA and *m*-Cu(BPA)-DNA. However, the

favorable (negative) intermolecular electrostatic interaction (ΔE_{ele}) is counteracted by the unfavorable (positive) polar solvation free energy ($\Delta G_{\text{pb/solv}}$). As a result, the total polar energies ($\Delta G_{\text{pb}} = \Delta E_{\text{ele}} + \Delta G_{\text{pb/solv}}$) are unfavorable for binding, with values of 16.9 and 12.3 $\text{kcal}\cdot\text{mol}^{-1}$ for adducts *p*-Cu(BPA)-DNA and *m*-Cu(BPA)-DNA formations, respectively. The entropic contribution ($T\Delta S$) was estimated by a normal-mode analysis and the results are included in Table 2. The solute entropy changes are found to be close to each other for the two nucleases because their structural properties are nearly identical. The solute entropic contributions ($T\Delta S$ values) are -24.0 and -22.3 $\text{kcal}\cdot\text{mol}^{-1}$ for the formation of *p*-Cu(BPA)-DNA and *m*-Cu(BPA)-DNA adducts, respectively. Summarily, these energy component analyses show that *m*-Cu(BPA) has a higher DNA-binding affinity than that of *p*-Cu(BPA), which is in agreement with the experimental results.⁴²

In addition, the hydrogen bonds analysis between nucleases and DNA also supports the above conclusions on DNA binding affinity. The occupancy and type of each of these hydrogen bond combinations are summarized in Table 3. The following can be seen: (1) For *p*-Cu(BPA)-DNA, there are three main hydrogen bonds whose occupancies are 71%, 52%, and 41%, respectively, two of them locate between C–H groups of sugars in DNA and N atoms on *p*-Cu(BPA), the third one locates between a N–H group on DNA base and an O atom on *p*-Cu(BPA). The lengths of the hydrogen bonds (C···N/C···N/N···O) are 3.61, 3.70, and 3.61 Å, respectively. There are a larger number of hydrogen bonds between *m*-Cu(BPA) and DNA base; these hydrogen bonds are generally stronger than those found in *p*-Cu(BPA)-DNA as well. The occupancies of the three main hydrogen bonds are 93%, 98%, and 53%, respectively; two of the hydrogen bonds locate between C–H groups of *m*-Cu(BPA) and O atoms in DNA bases, and the third one locates between an O atom of *m*-Cu(BPA) and the N–H group in DNA base. The distances of the three hydrogen bonds (C···O/C···O/N···O) are 3.43, 3.24, and 3.44 Å, respectively. (2) For *p*-Cu(BPA)-Pt-DNA and *m*-Cu(BPA)-Pt-DNA, we mainly compared the occupancies and lengths of the predominant hydrogen bonds. Take the two crucial hydrogen bonds between two C–H groups of *p*-Cu(BPA)-Pt with one O atom and one N atom of DNA base, for example, the lengths of the two hydrogen bonds (C···O and N···O) with the occupancies of 79% and 76% are 3.64 and 3.61 Å. For *m*-Cu(BPA)-Pt-DNA, there are two very strong hydrogen bonds between two O atoms of different bases of DNA and two C–H groups of *m*-Cu(BPA)-Pt. The lengths of the two hydrogen bonds (C···O and C···O) with the occupancies of 96% and 86% are 3.34 and 3.41 Å, respectively. In a word, the H-bonds in *m*-Cu(BPA)-DNA are stronger than those in *p*-Cu(BPA)-DNA, and the H-bonds in *m*-Cu(BPA)-Pt-DNA are stronger than those in *p*-Cu(BPA)-Pt-DNA, indicating that the interaction of *m*-Cu(BPA) with DNA is stronger than that of *p*-Cu(BPA) and the interaction of *m*-Cu(BPA)-Pt-DNA is stronger than that of *p*-Cu(BPA)-Pt-DNA.

Taken together, based on the results discussed above, the DNA binding affinities of the four nucleases are in the order of *p*-Cu(BPA) < *m*-Cu(BPA) < *p*-Cu(BPA)-Pt < *m*-Cu(BPA)-Pt, in agreement with the experiment.⁴²

3.2. DNA Cleavage Activity of Four Nucleases. Electrophoresis results of the DNA cleavage in experiment show the cleavage efficiency of the four nucleases follows an order of *p*-Cu(BPA) < *m*-Cu(BPA) < *p*-Cu(BPA)-Pt < *m*-

Table 3. Intermolecular Hydrogen Bonds in Four Adducts^a

<i>p</i> -Cu(BPA)-DNA		<i>m</i> -Cu(BPA)-DNA	
D-A ^a	occupancy ^b (%)	D-A	occupancy (%)
N _b –G ₆ /H4'-C4	71 (3.61) ^c	O–G ₆ /2H2-N2	98 (3.24)
N _b –C ₁₆ /H4'-C4	52 (3.70)	C ₁₆ /O4'-H-C _a	93 (3.43)
O–G ₅ /2H2-N2	41 (3.61)	T ₇ /O2–H-C _a	53 (3.44)
O–T ₇ /H5'1-C5	39 (3.79)	N _b –T ₇ /H5'1-C5	52 (3.47)
O–G ₆ /H4'-C4	38 (3.73)	G ₅ /O2–H-C _a	52 (3.68)
O–G ₆ /H1'-C1	26 (3.72)	C ₈ /O2–H-C _a	45 (3.74)
		N _b –C ₁₆ /H5'1-C5	44 (3.66)
		G ₅ /N2–H-C _a	41 (3.72)
		G ₅ /N3–H-C _a	39 (3.74)
		N _b –C ₁₆ /H4'-C4	39 (3.80)
		G ₆ /O4'-H-C _a	35 (3.43)
		C ₁₆ /O4'-H-C _a	33 (3.42)
		T ₇ /O4'-H-C _a	30 (3.29)
		G ₅ /N2–H-C _a	27 (3.80)
		T ₇ /O2–H-C _a	27 (3.74)
		N–C ₁₅ /H1'-C1	26 (3.84)
		C ₈ /O4'-H-C _a	23 (3.50)
		N _b –T ₇ /H4'-C4	21 (3.51)
<i>p</i> -Cu(BPA)-Pt-DNA		<i>m</i> -Cu(BPA)-Pt-DNA	
D-A	occupancy (%)	D-A	occupancy (%)
G ₁₈ /O5'-H-C _a	79 (3.64)	G ₅ /O6–H-C _a	96 (3.34)
G ₁₈ /N1–H-C _a	76 (3.61)	G ₁₈ /O4'-H-C _a	86 (3.41)
G ₅ /O4'-H-C _a	70 (3.57)	T ₄ /O2–H-C _a	76 (3.50)
G ₁₈ /N2–H-C _a	67 (3.60)	G ₆ /N7–H-C _a	71 (3.67)
G ₁₈ /N2–H-C _a	63 (3.64)	T ₄ /O4'-H-C _a	71 (3.40)
A ₁₇ /O3'-H-C _a	56 (3.36)	A ₁₇ /O4'-H-C _a	68 (3.48)
G ₅ /O4'-H-C _a	54 (3.50)	C ₃ /O2–H-C _a	64 (3.54)
G ₆ /O6–H-C _a	54 (3.47)	A ₁₇ /N3–H-C _a	59 (3.46)
G ₅ /N2–H-C _a	47 (3.74)	C ₁₆ /O2–H-C _a	55 (3.74)
G ₅ /N7–H-C _a	44 (3.84)	C ₁₆ /N3–H-C _a	41 (3.60)
T ₄ /O2–H-C _a	43 (3.16)	G ₅ /N7–H-C _a	41 (3.51)
T ₄ /O3'-H-C _a	38 (3.67)	G ₁₈ /N9–H-C _a	35 (3.57)
G ₁₈ /O4'-H-C _a	37 (3.50)	G ₁₈ /N7–H-C _a	34 (3.73)
T ₄ /O4'-H-C _a	36 (3.84)	G ₁₈ /N2–H-C _a	30 (3.66)
T ₄ /O3'-H-C _a	33 (3.74)	N _b –G ₁₈ /H5'2-C5	30 (3.70)
G ₅ /O5'-H-C _a	30 (3.81)	G ₁₈ /O6–H-C _a	29 (3.57)
C ₃ /N4–H-C _a	25 (3.66)	G ₅ /N3–H-C _a	27 (3.84)
T ₄ /O2–H-C _a	20 (3.40)	G ₁₈ /N7–H-C _a	24 (3.74)
		G ₅ /O5'-H-C _a	24 (3.70)
		G ₅ /O5'-H-C _a	23 (3.78)
		C ₃ /N4–H-C _a	23 (3.71)
		G ₁₈ /N9–H-C _a	23 (3.64)
		G ₁₈ /N3–H-C _a	22 (3.52)

^aD-A: donor atom–acceptor atom. ^bThe percentage of time that the hydrogen bond is observed during the trajectory; hydrogen bonds are reported only if they exist for more than 20% of the investigated time period. ^cValues in parentheses are distances of acceptor–donor atoms.

^dN_b: sp² hybridized nitrogen atom. O: sp² hybridized oxygen atom. C_a: aromatic carbon atom.

Cu(BPA)-Pt.⁴² Many of the metallonucleases are known to cleave the DNA strand by oxidative/reductive pathways.^{73–75} The redox process causing DNA strand scission often occurs via abstraction of H1', H4', H5'1, or H5'2 of DNA sugar by nucleases in the presence of oxidative/reductive agents.^{76–78} To address the observed different cleavage activities of the four nucleases in the experiment,⁴² the probability distributions of the distances between the copper center of nuclease and H1', H4', H5'1, or H5'2 atoms of the nearest sugar in the DNA

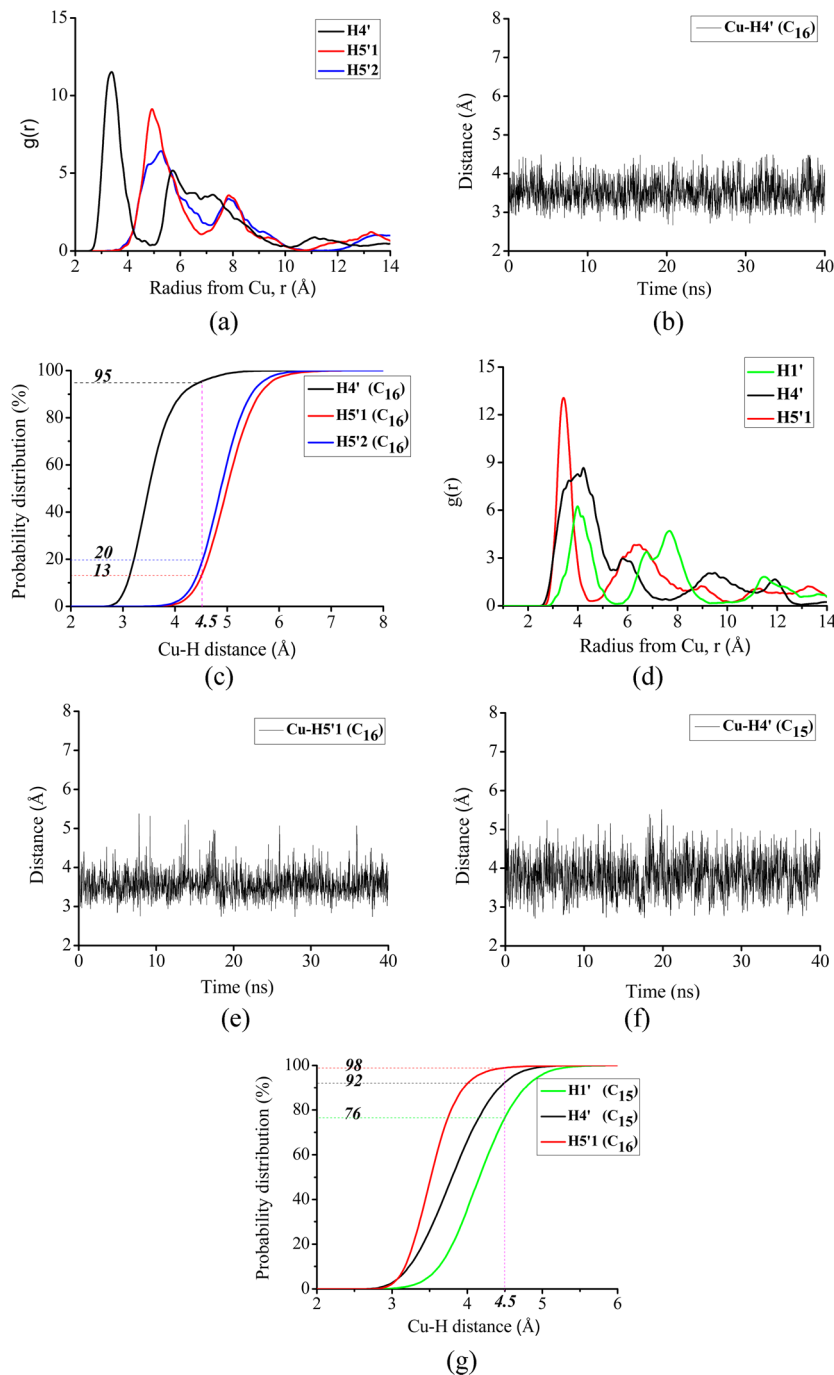


Figure 2. RDF curves of copper–hydrogen, Cu–H distances, and probability distributions of Cu–H: (a)/(b)/(c) for *p*-Cu(BPA)-DNA and (d)/(e),(f)/(g) for *m*-Cu(BPA)-DNA.

molecule for each adduct have been analyzed in detail. The radial distribution function (RDF) has been widely used to describe the structure characterization of the condensation phase, and the RDF between the Cu atom and the H atom of sugar may provide primary information regarding the DNA strand scission possibility. Therefore, the RDFs between the copper center of the nuclease and the hydrogen atoms of the DNA sugar are discussed in the following section.

3.2.1. Cleavage Activities of *p*-Cu(BPA) and *m*-Cu(BPA). The RDFs, distances of Cu–H, and probability distributions of Cu–H distances are presented in parts a–c of Figure 2 for *p*-Cu(BPA)-DNA and parts d–g of Figure 2 for *m*-Cu(BPA)-DNA. For *p*-Cu(BPA)-DNA, Figure 2a shows that the first

sharp RDF peaks of Cu–H4', Cu–H5'1, and Cu–H5'2 are centered at 3.51, 4.83, and 5.23 Å, respectively, indicating that the possibility of the H4' abstraction is higher than that of H5'1 and H5'2. Figure 2b shows that the average distance between Cu and H4' of the nearest sugar is 3.51 Å, which supports the DNA cleavage mechanisms by metallonucleases proposed by some experimental^{16,79,80} and theoretical^{28,43–49} studies. On the basis of a previously proposed DNA-cleavage mechanism,⁸¹ the average distance between the copper center and the hydrogen atom of sugar, 4.50 Å, which is appropriate for inserting a substrate for a redox procedure, is selected as a cutoff criterion in this work. Figure 2c shows that the probability distribution of the Cu–H4' distance is less than

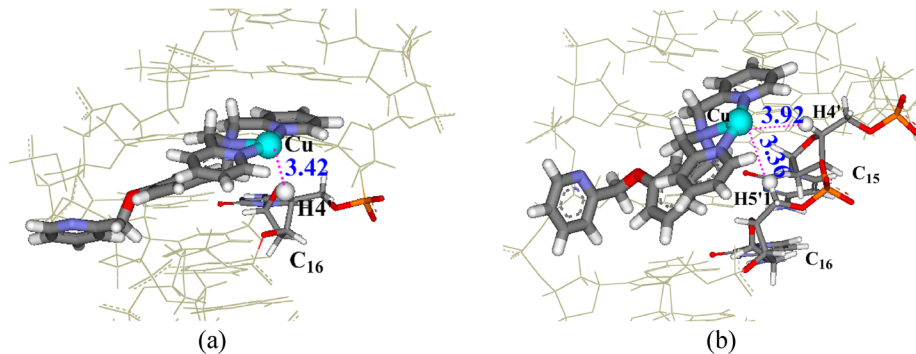


Figure 3. Local average structures of (a) *p*-Cu(BPA)-DNA and (b) *m*-Cu(BPA)-DNA and the average distances between copper (in cyan) and hydrogen atoms (in white).

4.50 Å for 95% of the simulation time and the probability distributions of Cu–H5'1 and Cu–H5'2 distances are less than 4.50 Å for only 13% and 20% of the simulation time, respectively, which supports the conclusion that the H4' abstraction by *p*-Cu(BPA) is favored over that of H5'1 and H5'2. For *m*-Cu(BPA)-DNA, Figure 2d shows that the first RDF peaks of Cu–H5'1, Cu–H4', and Cu–H1' are centered at 3.50, 3.73, and 4.13 Å, respectively. The average distances between the Cu and H5'1/H4' of the nearest sugar are about 3.50 and 3.73 Å as shown in parts e and f of Figure 2. Figure 2g presents the probability distributions of the Cu–H5'1, Cu–H4', and Cu–H1' distances, which are less than 4.50 Å for 98%, 92%, and 76% of the simulation time, respectively. The results of probability distributions indicate that the H5'1 abstraction by the copper center for *m*-Cu(BPA)-DNA is more favorable. Collectively, DNA strands cleaved by *p*-Cu(BPA)/*m*-Cu(BPA) could occur via hydrogen abstractions from sugar. Namely, the DNA strand scission caused by *p*-Cu(BPA) occurs at the nearest base (C_{16}) while the DNA strand cleavage could occur at two adjacent bases ($C_{15}C_{16}$) for the *m*-Cu(BPA)-DNA system, indicating that the DNA cleavage sequence specificity of *p*-Cu(BPA) is higher than that of *m*-Cu(BPA). The distance probability distributions suggest that the cleavage activity of *m*-Cu(BPA) is higher than that of *p*-Cu(BPA).

The visual structural analyses for *p*-Cu(BPA)-DNA and *m*-Cu(BPA)-DNA reveal details of the interaction of *p*-Cu(BPA)/*m*-Cu(BPA) with DNA. The average structure of *p*-Cu(BPA)-DNA (shown in Figure 3a) demonstrates that the DNA cleavage probably occurs when the Cu atom of *p*-Cu(BPA) abstracts the H4' of the nearest deoxyribose sugar linking to C_{16} base, with an average Cu–H4' distance of 3.42 Å. For *m*-Cu(BPA), the different orientations of $[Cu(BPA)]^{2+}$ moiety lead to more cleavage possibilities. Specifically, Figure 3b demonstrates that the copper atom of *m*-Cu(BPA) could abstract H5'1 of the deoxyribose sugar linking to C_{16} base as well as H4' of the deoxyribose sugar linking to C_{15} base, with average Cu–H5'1 and Cu–H4' distances of 3.36 and 3.92 Å, respectively. These structural characteristics reveal theoretically the random DNA cleavage activities of *m*-Cu(BPA) determined by its floating locations in the minor groove.

3.2.2. Cleavage Activities of *p*-Cu(BPA)-Pt and *m*-Cu(BPA)-Pt. To investigate DNA cleavage activities of dinuclear nucleases, the RDFs, distances of Cu–H, and probability distributions of Cu–H distances are calculated and shown in parts a/b,c/d of Figure 4 for *p*-Cu(BPA)-Pt-DNA and parts e/f,g/h for Figure 4 for *m*-Cu(BPA)-Pt-DNA, respectively. For *p*-Cu(BPA)-Pt-DNA, Figure 4a shows that the first sharp RDF

peaks of Cu–H5'1, Cu–H4', and Cu–H5'2 are centered at 3.48, 4.12, and 4.64 Å, respectively. The average distances of Cu–H5'1 and Cu–H4' are 3.48 and 5.01 Å in the first 10 ns of the simulation and are 5.01 and 4.12 Å in 10–40 ns of the simulation as shown in Figure 4b/c, suggesting that the copper center moves from H5'1 to H4' along the time frame of the simulation. In addition, Figure 4d presents the probability distributions of the Cu–H5'1, Cu–H4', and Cu–H5'2 distances, which are less than 4.50 Å for 23%, 72%, and 28% of the simulation time, respectively, indicating that H4' abstraction by *p*-Cu(BPA)-Pt is more favorable than that of H5'2. For *m*-Cu(BPA)-Pt-DNA, the first sharp RDF peaks of Cu–H5'2, Cu–H5'1, and Cu–H4' are centered at 3.41, 4.28, and 5.34 Å, respectively (as shown in Figure 4e). The average distances of Cu–H5'2 and Cu–H5'1 are 3.41 and 4.28 Å, respectively, suggesting that the H5'2 abstraction by *m*-Cu(BPA)-Pt is preferable to that of H5'1 (see Figure 4f/g). Figure 4h presents the probability distributions of the Cu–H5'2 and Cu–H5'1 distances, which are less than 4.50 Å for 82% and 54% of the simulation time, respectively, which also indicate that the H5'2 abstraction is more favorable than that of H5'1 in the *m*-Cu(BPA)-Pt-DNA system. Note that sudden change appears in the Cu–H distance of *p*-Cu(BPA)-Pt-DNA in Figure 4b/c but not in *m*-Cu(BPA)-Pt-DNA; this could be due to there being a larger number and stronger H-bonds in *m*-Cu(BPA)-Pt-DNA than those in *p*-Cu(BPA)-Pt-DNA (discussed in Section 3.1, Binding Affinity of Four Nucleases). In addition, for *p*-Cu(BPA)-Pt-DNA, visual analyses of corresponding snapshots show that the angle between the plane of $[Cu(BPA)]^{2+}$ and the wall of the minor groove changed from about 60° to 90° from first 10 ns to 10–40 ns. These different orientations of the $[Cu(BPA)]^{2+}$ moiety in *p*-Cu(BPA)-Pt-DNA may contribute to the sudden change of the Cu–H distance.

On the basis of the results mentioned above, hydrogen abstraction by *m*-Cu(BPA)-Pt is more favorable than that by *p*-Cu(BPA)-Pt. The distance analyses verified the stability of the copper moiety of *p*-Cu(BPA)-Pt and *m*-Cu(BPA)-Pt in the minor groove of DNA, which makes all possible abstracted hydrogen atoms from only one deoxyribose sugar linking to G_{18} base. However, as discussed earlier, the mononuclear nuclease of *m*-Cu(BPA) could abstract different hydrogen atoms from two adjacent deoxyribose sugars linking to C_{15} and C_{16} bases, respectively. The present observations indicate that it is possible for the dinuclear nucleases to specifically abstract hydrogen atoms from only one sugar of DNA. That is, dinuclear nucleases, *p*-Cu(BPA)-Pt/*m*-Cu(BPA)-Pt, have better

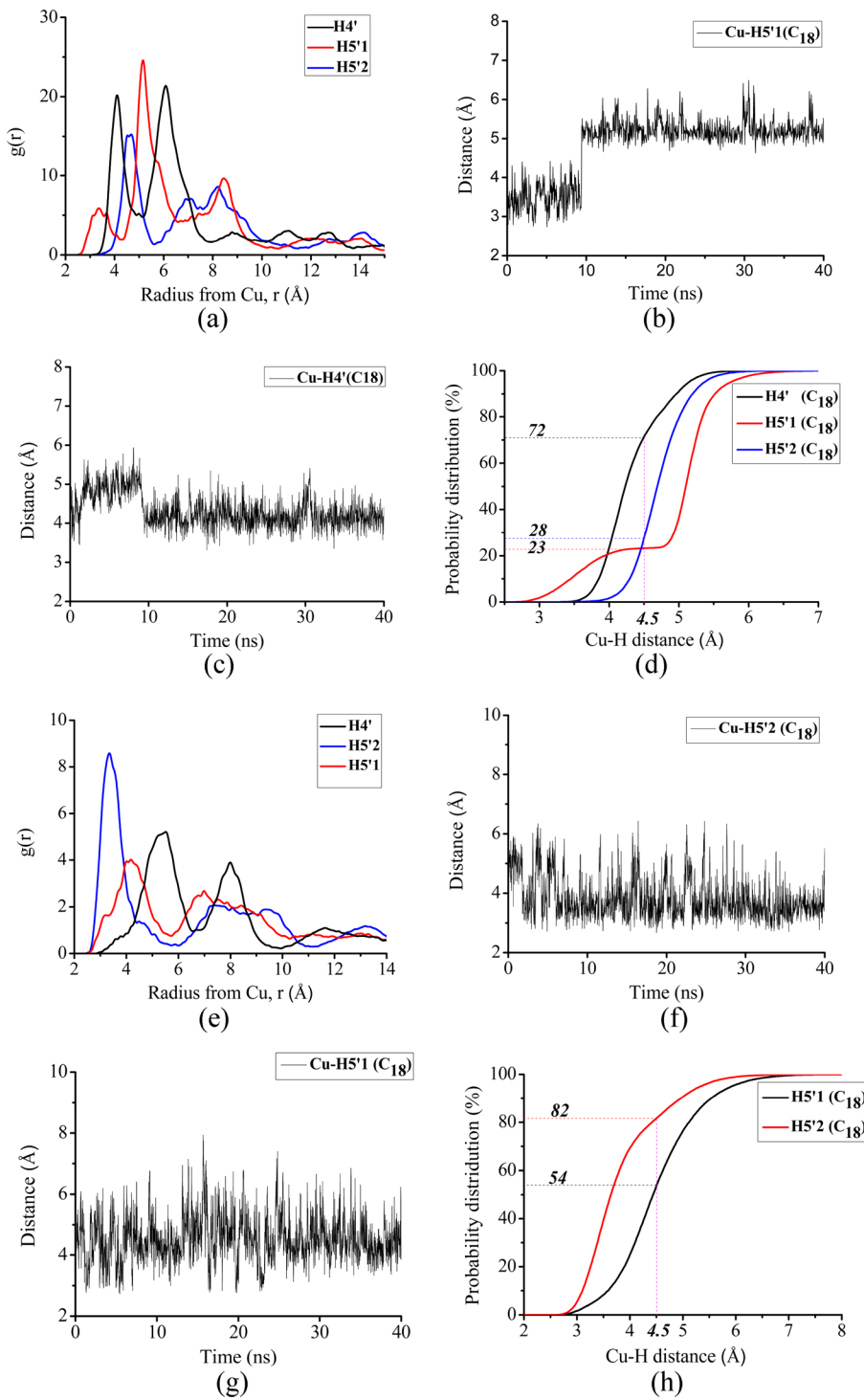


Figure 4. RDF curves of copper–hydrogen, Cu–H distances, and probability distributions of Cu–H distance: (a)/(b),(c)/(d) for *p*-Cu(BPA)-Pt-DNA and (e)/(f),(g)/(h) for *m*-Cu(BPA)-Pt-DNA.

sequence-selectivity for cleavage of DNA compared with mononuclear nuclease *m*-Cu(BPA).

Visual analyses of the trajectories for *p*-Cu(BPA)-Pt-DNA and *m*-Cu(BPA)-Pt-DNA reveal details of the interaction of nuclease with DNA in each system. The plane of [Cu(BPA)]²⁺ of *p*-Cu(BPA)-Pt in the first 10 ns of the simulation locates in the minor groove of DNA with the angle of about 60° between the plane of [Cu(BPA)]²⁺ and the wall of the minor groove, the average distance of Cu with H5'1 of the nearest sugar linking to G₁₈ base is 3.49 Å (shown in Figure 5a). In 10–40 ns of the

simulation, the plane of [Cu(BPA)]²⁺ in *p*-Cu(BPA)-Pt became almost vertical to the wall of the DNA minor groove and the average distance of Cu–H4' is 4.19 Å in Figure 5b. Therefore, the different orientations of [Cu(BPA)]²⁺ provide the possibility of *p*-Cu(BPA)-Pt abstracting different hydrogen atoms from the same sugar as observed above. For *m*-Cu(BPA)-Pt-DNA, the plane of [Cu(BPA)]²⁺ is parallel to the wall of the minor groove of DNA during the time frame of the simulation, and the Cu atom of *m*-Cu(BPA)-Pt approaches the

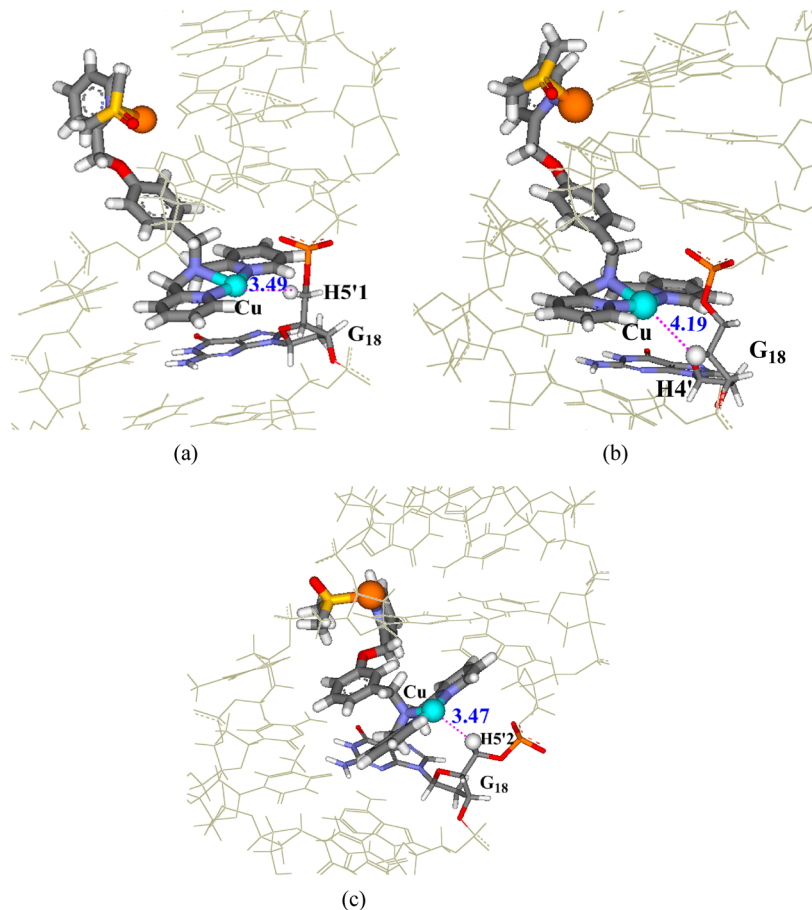


Figure 5. Local average structures of *p*-Cu(BPA)-Pt-DNA and *m*-Cu(BPA)-Pt-DNA along with the distances between copper (in cyan) and hydrogen (in white): (a) *p*-Cu(BPA)-Pt-DNA in the first 10 ns simulation, (b) *p*-Cu(BPA)-Pt-DNA in the 10–30 ns simulation, and (c) *m*-Cu(BPA)-Pt-DNA.

H5'2 atom of the nearest sugar linking to G₁₈ base with an average Cu–H5'2 distance of 3.47 Å, as presented in Figure 5c.

3.3. Analysis of DNA Conformational Dynamics and Groove Parameters. The base pair and base pair step helical parameters of *p*-Cu(BPA)/*m*-Cu(BPA)-DNA are only slightly different from those of the B-DNA molecule as shown in Figure S3 in the Supporting Information; therefore, we will not discuss this information in this work. Cases in which the frequency distributions of DNA helical parameters of copper–platinum–DNA adduct are tremendously different from those of the canonical B-DNA are shown in Figure 6. Profiles of frequency distributions of the base pair parameters for *p*-Cu(BPA)-Pt-DNA and *m*-Cu(BPA)-Pt-DNA shifted extensively from those for the undamaged B-DNA, implying that *p*-Cu(BPA)-Pt/*m*-Cu(BPA)-Pt make the large conformational flexibility of DNA backbones. The differences of base pair parameters include the propeller for C₃-G₁₈ base pair and propeller/buckle/shear for T₄-A₁₇ base pair; in addition, the comparisons show significant differences in the shift for C₃/T₄ and T₄/G₅ base pair steps and the twist/roll for C₃/T₄, T₄/G₅, and G₅/G₆ base pair steps, indicating that the conformational dynamics profile of B-DNA is altered obviously by dinuclear nucleases of *p*-Cu(BPA)-Pt/*m*-Cu(BPA)-Pt. It is worth noting that the *p*-Cu(BPA)-Pt/*m*-Cu(BPA)-Pt-DNA show more significant differences in the frequency distributions of the DNA helical parameters from the undamaged B-DNA than *p*-Cu(BPA)/*m*-Cu(BPA)-DNA, which makes it more difficult for DNA repair by *p*-Cu(BPA)-

Pt/*m*-Cu(BPA)-Pt as well as gene transcription. Especially, the distortion of the DNA conformation induced by *m*-Cu(BPA)-Pt from that by *p*-Cu(BPA)-Pt is more serious.

Visual analyses of DNA structures of each adduct during the simulation support the simulated results mentioned above. Superposition of the average structures of damaged DNA by *p*-Cu(BPA)-Pt and *m*-Cu(BPA)-Pt with the undamaged B-DNA molecule are shown, respectively, in parts a and b of Figure 7. The damaged DNA conformation, including the bending motion, unwinding extent, and twisting degree, shows obvious differences from the undamaged B-DNA conformation. Specifically, (1) the DNA backbone bending is clearly presented for both adducts, *p*-Cu(BPA)-Pt-DNA/*m*-Cu(BPA)-Pt-DNA. (2) The DNA double-strand unwinding in the vicinity of the binding sites leads to a large change to the DNA groove conformation with respect to the undamaged B-DNA molecule, which makes it more difficult for DNA repair as well as gene transcription. (3) The twisting motions cause some bases to fray away from the groove, and make the DNA structures in adducts significantly distort from a canonical B-DNA. Moreover, it is observed that the distortions of DNA conformations induced by *m*-Cu(BPA)-Pt are larger than those by *p*-Cu(BPA)-Pt.

The DNA structural deformations are frequently associated with changes in the groove width and depth. Therefore, the minor groove width and depth of DNA in *p*-Cu(BPA)-Pt/*m*-Cu(BPA)-Pt-DNA were also calculated to study the effect of *p*-

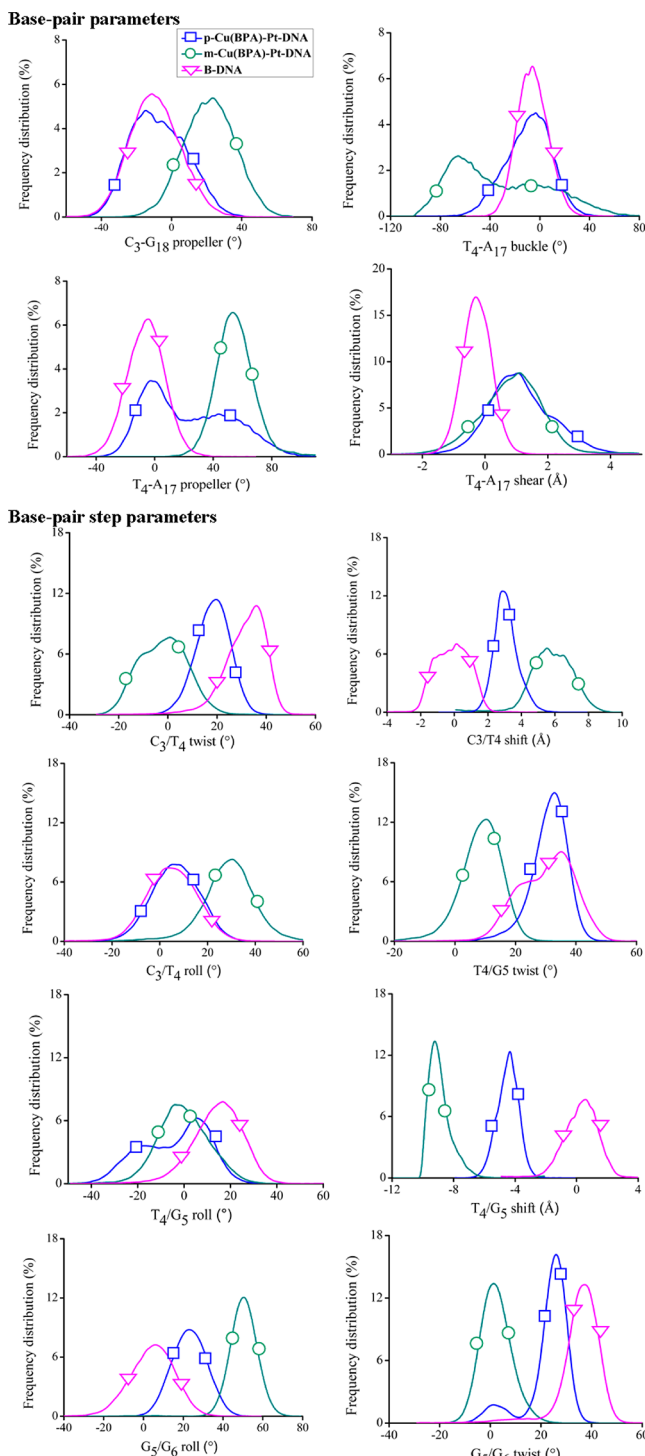


Figure 6. Frequency distributions of representative DNA duplex helical parameters for the four successive base pairs $C_3-T_4-G_5-G_6$: B-DNA (magenta lines with down-triangle); $p\text{-Cu(BPA)\text{-Pt-DNA}}$ (blue lines with square); and $m\text{-Cu(BPA)\text{-Pt-DNA}}$ (green lines with cycle). (The diverse symbols were used to distinguish the different curves and do not refer to the true data.)

$\text{Cu(BPA)\text{-Pt}}$ and $m\text{-Cu(BPA)\text{-Pt}}$ on DNA conformations. Parts a and b of Figure 8 compare the minor groove widths and depths of the $p\text{-Cu(BPA)\text{-Pt}}/m\text{-Cu(BPA)\text{-Pt-DNA}}$ with an undamaged B-DNA. The reported minor groove widths and depths are respectively averages of the widths and depths from each snapshot of all trajectories. An undamaged and canonical

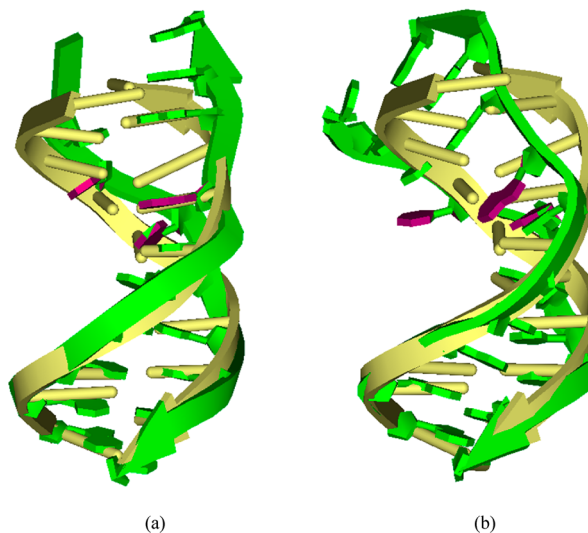


Figure 7. Superpositions of average structures between B-DNA (yellow) and damaged DNA (green) in (a) $p\text{-Cu(BPA)\text{-Pt-DNA}}$ and (b) $m\text{-Cu(BPA)\text{-Pt-DNA}}$. (Red bases refer to fraying bases.)

B-DNA has an average minor groove width of 5.87 \AA and depth of 4.64 \AA .⁸² It is obvious from parts a and b of Figure 8 that the minor groove widths and depths change the most significantly at or near the binding sites with respect to the undamaged B-DNA. Especially, as the minor groove increases its width, the corresponding depths become shallow. For instance, for $m\text{-Cu(BPA)\text{-Pt-DNA}}$, the minor groove widths of DNA are greatly widened by 57% (from 5.87 to 9.22 \AA), 95% (from 5.87 to 11.47 \AA), and 88% (from 5.87 to 11.05 \AA) at the $T_4\text{-A}_{17}$, $G_5\text{-C}_{16}$, and $G_6\text{-C}_{15}$ base pairs, respectively. Their corresponding minor groove depths are shallowed by 36% (from 4.64 to 2.95 \AA), 92% (from 4.64 to 0.39 \AA), and 67% (from 4.64 to 1.51 \AA), respectively. For $p\text{-Cu(BPA)\text{-Pt-DNA}}$, the minor groove widths at $T_4\text{-A}_{17}$, $G_5\text{-C}_{16}$, and $G_6\text{-C}_{15}$ of DNA are widened by 31% (from 5.87 to 7.67 \AA), 23% (from 5.87 to 7.21 \AA), and 10% (from 5.87 to 6.46 \AA) and the corresponding minor groove depths are shallowed by 27% (from 4.64 to 3.37 \AA), 19% (from 4.64 to 3.77 \AA), and 0.44% (from 4.64 to 4.62 \AA) compared with the normal B-DNA. The minor groove widths and depths calculated by the time-averaged structure are also shown in the Supporting Information (see Figure S4). These observations demonstrate the fact that the distortion of the DNA conformation is more seriously induced by $m\text{-Cu(BPA)\text{-Pt}}$ than by $p\text{-Cu(BPA)\text{-Pt}}$.

To assess the stability of the DNA duplex, for $p\text{-Cu(BPA)\text{-Pt-DNA}}$ and $m\text{-Cu(BPA)\text{-Pt-DNA}}$, the occupancy of all possible hydrogen bonds between base pairs (calculated as the percentage of the time that the hydrogen bonds existed during the simulation) was measured along with B-DNA as shown in Figure 8c. When compared to B-DNA, both damaged DNA molecules show a substantial decrease in standard Watson–Crick hydrogen bond occupancy at the $C_3\text{-G}_{18}$, $T_4\text{-A}_{17}$, $G_5\text{-C}_{16}$, $G_6\text{-C}_{15}$, $T_7\text{-A}_{14}$, and $C_8\text{-G}_{13}$ base pairs, whereas the base pairs of B-DNA are almost completely intact. These observations demonstrate that the distortions of the DNA duplexes influenced by $p\text{-Cu(BPA)\text{-Pt}}/m\text{-Cu(BPA)\text{-Pt}}$ in the vicinity of the platination sites are significant, which could result in real damage to the original DNA structure.

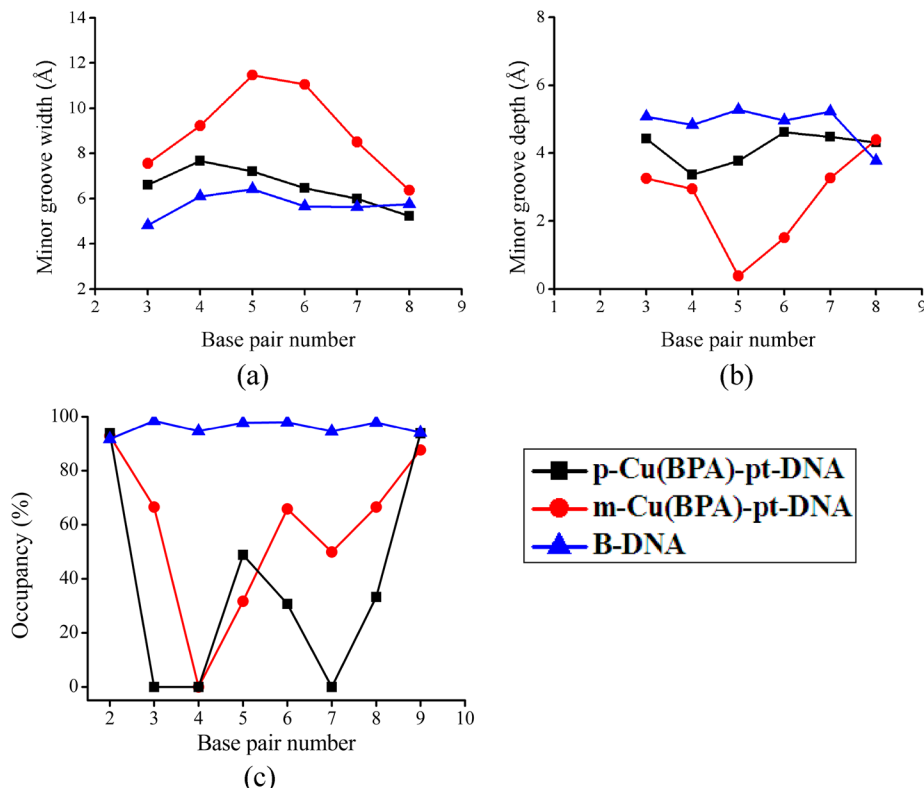


Figure 8. (a/b) Minor groove widths and depths of the DNA conformations calculated by averaging every snapshot parameter. (c) The standard Watson–Crick hydrogen bond occupancies of base pairs in B-DNA, *p*-Cu(BPA)-Pt-DNA, and *m*-Cu(BPA)-Pt-DNA. B-DNA (blue line with up-triangle), *p*-Cu(BPA)-Pt-DNA (black line with square), and *m*-Cu(BPA)-Pt-DNA (red line with circle).

4. CONCLUSIONS

Molecular dynamics simulations for four nuclelease–DNA adducts, including two copper–DNA (*p*-Cu(BPA)-DNA and *m*-Cu(BPA)-DNA) adducts and two copper–platinum–DNA (*p*-Cu(BPA)-Pt-DNA and *m*-Cu(BPA)-Pt-DNA) adducts, were performed to investigate the binding affinity and cleavage activity of four nucleases and to address that the platinum center plays a vital role for dinuclear nucleases in binding affinity and efficient sequence-specific cleavage. The obtained results demonstrated that the DNA binding affinity of the four nucleases is in the order of *p*-Cu(BPA) < *m*-Cu(BPA) < *p*-Cu(BPA)-Pt < *m*-Cu(BPA)-Pt, which mainly results from intermolecular binding modes and the intermolecular hydrogen bonds formations, in accord with the experimental results.⁴² The results of distance probability distributions calculation indicate that hydrogen atoms of sugar could be abstracted by *p*-Cu(BPA), *m*-Cu(BPA), *p*-Cu(BPA)-Pt, and *m*-Cu(BPA)-Pt. Abstraction of these hydrogen atoms leads either to radicals centered on the sugar carbon or to lesion nucleosides, respectively, and ultimately DNA strand scission.⁸³ The results of the current investigation agree well with the efficiencies of DNA selective cleavage ability observed experimentally: introduction of two metal centers for dinuclear nucleases has improved not only their DNA binding affinities but also DNA cleavage specificities. Moreover, the simulated results demonstrate that the extent of DNA conformational distortions induced by dinuclear nucleases is greater than those by mononuclear nucleases. Specifically, *p*-Cu(BPA)-Pt/*m*-Cu(BPA)-Pt can significantly facilitate DNA conformational distortion, predicting the dinuclear nucleases exhibit the improved nuclease activities compared with their mononuclear

counterparts. The present study provides useful information to better understand the interactions of the different nucleases with DNA and could provide some theoretical instructions in designing of more effective DNA cleavers.

ASSOCIATED CONTENT

Supporting Information

Figures S1–S4 and the protocol of MD simulations; details of atom types of the four studied nucleases, RMSD of all backbone atoms, frequency distributions of DNA duplex helical parameters for some representative base pairs for mononuclear adducts *p*-Cu(BPA)-DNA and *m*-Cu(BPA)-DNA, and minor groove widths and depths for the time-averaged structure parameters of the DNA conformations. This material is available free of charge via the Internet at <http://pubs.acs.org>.

AUTHOR INFORMATION

Corresponding Author

*E-mail: zhuyan@zzu.edu.cn (Y.Y.Z.) and mstang@zzu.edu.cn (M.S.T.).

Notes

The authors declare no competing financial interest.

ACKNOWLEDGMENTS

We are grateful to Dr. Xiaonan Tang for his valuable suggestions on language. The authors acknowledge financial support from the National Natural Science Foundation of China (No. 21001095), China Postdoctoral Science Foundation (No. 20100480858), and Training Foundation of Zhengzhou University for Innovation & Enterprise Capability of College Student (No. 2011cxsy046).

■ REFERENCES

- (1) Gonzalez-Alvarez, M.; Alzuet, G.; Borras, J.; Pitie, M.; Meunier, B. *J. Biol. Inorg. Chem.* **2003**, *8*, 644–652.
- (2) Jiang, Q.; Xiao, N.; Shi, P. F.; Zhu, Y. G.; Guo, Z. *J. Coord. Chem. Rev.* **2007**, *251*, 1951–1972.
- (3) Boerner, L. J. K.; Zaleski, J. M. *Curr. Opin. Chem. Biol.* **2005**, *9*, 135–144.
- (4) Cowan, J. A. *Curr. Opin. Chem. Biol.* **2001**, *5*, 634–642.
- (5) Morrow, J. R.; Iranzo, O. *Curr. Opin. Chem. Biol.* **2004**, *8*, 192–200.
- (6) Tonde, S. S.; Kumbhar, A. S.; Padhye, S. B.; Butcher, R. J. *J. Inorg. Biochem.* **2006**, *100*, 51–57.
- (7) Drewry, J. A.; Gunning, P. T. *Coord. Chem. Rev.* **2011**, *255*, 459–472.
- (8) Pitié, M.; Boldron, C.; Pratviel, G. *Adv. Inorg. Chem.* **2006**, *58*, 77–130.
- (9) Bal, W.; Kasprzak, K. S. *Toxicol. Lett.* **2002**, *127*, 55–62.
- (10) Oivanen, M.; Kuusela, S.; Lönnberg, H. *Chem. Rev.* **1998**, *98*, 961–990.
- (11) Thederahn, T. B.; Kuwabara, M. D.; Larsen, T. A.; Sigman, D. S. *J. Am. Chem. Soc.* **1989**, *111*, 4941–4946.
- (12) Pratviel, G.; Bernadou, J.; Meunier, B. *Angew. Chem., Int. Ed.* **1995**, *34*, 746–769.
- (13) Sitlani, A.; Long, E. C.; Pyle, A. M.; Barton, J. K. *J. Am. Chem. Soc.* **1992**, *114*, 2303–2312.
- (14) Pitie, M.; Meunier, B. *Bioconjugate Chem.* **1998**, *9*, 604–611.
- (15) Schweigert, N.; Acero, J. L.; von Gunten, U.; Canonica, S.; Zehnder, A. J. B.; Eggen, R. I. L. *Environ. Mol. Mutagen.* **2000**, *36*, 5–12.
- (16) Pitié, M.; Boldron, C.; Gornitzka, H.; Hemmert, C.; Donnadieu, B.; Meunier, B. *Eur. J. Inorg. Chem.* **2003**, *2003*, 528–540.
- (17) Garcia-Raso, A.; Fiol, J. J.; Adrover, B.; Moreno, V.; Mata, I.; Espinosa, E.; Molins, E. *J. Inorg. Biochem.* **2003**, *95*, 77–86.
- (18) Barceló-Olivier, M.; García-Raso, Á.; Terrón, Á.; Molins, E.; Prieto, M. J.; Moreno, V.; Martínez, J.; Lladó, V.; López, I.; Gutiérrez, A.; et al. *J. Inorg. Biochem.* **2007**, *101*, 649–659.
- (19) Barve, A.; Kumbhar, A.; Bhat, M.; Joshi, B.; Butcher, R.; Sonawane, U.; Joshi, R. *Inorg. Chem.* **2009**, *48*, 9120–9132.
- (20) Chikira, M.; Tomizawa, Y.; Fukita, D.; Sugizaki, T.; Sugawara, N.; Yamazaki, T.; Sasano, A.; Shindo, H.; Palaniandavar, M.; Antholine, W. E. *J. Inorg. Biochem.* **2002**, *89*, 163–173.
- (21) Selvakumar, B.; Rajendiran, V.; Uma Maheswari, P.; Stoeckli-Evans, H.; Palaniandavar, M. *J. Inorg. Biochem.* **2006**, *100*, 316–330.
- (22) Dhar, S.; Reddy, P. A. N.; Nethaji, M.; Mahadevan, S.; Saha, M. K.; Chakravarty, A. R. *Inorg. Chem.* **2002**, *41*, 3469–3476.
- (23) Maheswari, P. U.; Lappalainen, K.; Sfregola, M.; Barends, S.; Gamez, P.; Turpeinen, U.; Mutikainen, I.; van Wezel, G. P.; Reedijk, J. *Dalton Trans.* **2007**, 3676–3683.
- (24) Oikawa, S.; Kawanishi, S. *Biochemistry* **1996**, *35*, 4584–4590.
- (25) Bales, B. C.; Kodama, T.; Weledji, Y. N.; Pitie, M.; Meunier, B.; Greenberg, M. M. *Nucleic Acids Res.* **2005**, *33*, 5371–5379.
- (26) Humphreys, K. J.; Karlin, K. D.; Rokita, S. E. *J. Am. Chem. Soc.* **2001**, *123*, 5588–5589.
- (27) Humphreys, K. J.; Johnson, A. E.; Karlin, K. D.; Rokita, S. E. *J. Biol. Inorg. Chem.* **2002**, *7*, 835–842.
- (28) Zhu, Y. Y.; Wang, Y.; Chen, G. *J. J. Phys. Chem. B* **2009**, *113*, 839–848.
- (29) de Hoog, P.; Louwerse, M. J.; Gamez, P.; Pitie, M.; Baerends, E. J.; Meunier, B.; Reedijk, J. *Eur. J. Inorg. Chem.* **2008**, 612–619.
- (30) Pitie, M.; Sudres, B.; Meunier, B. *Chem. Commun.* **1998**, 2597–2598.
- (31) Pitie, M.; Van Horn, J. D.; Brion, D.; Burrows, C. J.; Meunier, B. *Bioconjugate Chem.* **2000**, *11*, 892–900.
- (32) Pitie, M.; Burrows, C. J.; Meunier, B. *Nucleic Acids Res.* **2000**, *28*, 4856–4864.
- (33) Pitie, M.; Croisy, A.; Carrez, D.; Boldron, C.; Meunier, B. *ChemBioChem* **2005**, *6*, 686–691.
- (34) Boldron, C.; Ross, S. A.; Pitie, M.; Meunier, B. *Bioconjugate Chem.* **2002**, *13*, 1013–1020.
- (35) Frey, S. T.; Sun, H. H. J.; Murthy, N. N.; Karlin, K. D. *Inorg. Chim. Acta* **1996**, *242*, 329–338.
- (36) Chen, J.; Wang, X.; Shao, Y.; Zhu, J.; Zhu, Y.; Li, Y.; Xu, Q.; Guo, Z. *Inorg. Chem.* **2007**, *46*, 3306–3312.
- (37) Humphreys, K. J.; Karlin, K. D.; Rokita, S. E. *J. Am. Chem. Soc.* **2002**, *124*, 8055–8066.
- (38) Thyagarajan, S.; Murthy, N. N.; Sarjeant, A. A. N.; Karlin, K. D.; Rokita, S. E. *J. Am. Chem. Soc.* **2006**, *128*, 7003–7008.
- (39) de Hoog, P.; Boldron, C.; Gamez, P.; Slidregt-Bol, K.; Roland, I.; Pitie, M.; Kiss, R.; Meunier, B.; Reedijk, J. *J. Med. Chem.* **2007**, *50*, 3148–3152.
- (40) de Hoog, P.; Pitié, M.; Amadei, G.; Gamez, P.; Meunier, B.; Kiss, R.; Reedijk, J. *J. Biol. Inorg. Chem.* **2008**, *13*, 575–586.
- (41) Özalp-Yaman, Ş.; de Hoog, P.; Amadei, G.; Pitié, M.; Gamez, P.; Dewelle, J.; Mijatovic, T.; Meunier, B.; Kiss, R.; Reedijk, J. *Chem.—Eur. J.* **2008**, *14*, 3418–3426.
- (42) Dong, X. D.; Wang, X. Y.; Lin, M. X.; Sun, H.; Yang, X. L.; Guo, Z. *J. Inorg. Chem.* **2010**, *49*, 2541–2549.
- (43) Zhu, Y. Y.; Chen, Z. F.; Guo, Z. J.; Wang, Y.; Chen, G. *J. J. Mol. Model.* **2009**, *15*, 469–479.
- (44) Zhu, Y. Y.; Su, Y. W.; Li, X. C.; Wang, Y.; Chen, G. *J. Chem. Phys. Lett.* **2008**, *455*, 354–360.
- (45) Zhu, Y. Y.; Wang, Y.; Chen, G. J.; Zhan, C. G. *Theor. Chem. Acc.* **2009**, *122*, 167–178.
- (46) Robertazzi, A.; Vargiu, A. V.; Magistrato, A.; Ruggerone, P.; Carloni, P.; de Hoog, P.; Reedijk, J. *J. Phys. Chem. B* **2009**, *113*, 10881–10890.
- (47) Zhu, Y. Y.; Wang, Y.; Chen, G. *J. Nucleic Acids Res.* **2009**, *37*, 5930–5942.
- (48) Yue, H. W.; Zhu, Y. Y.; Wang, Y.; Chen, G. *BMC Struct. Biol.* **2010**, *10*, 1–14.
- (49) Wang, Y. R.; Zhu, Y. Y.; Wang, Y.; Chen, G. *J. Mol. Recognit.* **2011**, *24*, 981–994.
- (50) Frisch, M. J.; Trucks, G. W.; Schlegel, H. B.; Scuseria, G. E.; Robb, M. A.; Cheeseman, J. R.; Scalmani, G.; Barone, V.; Mennucci, B.; Petersson, G. A.; et al. *GAUSSIAN 09*, Revision C.01; Gaussian, Inc.: Wallingford, CT, 2010.
- (51) Becke, A. D. *J. Chem. Phys.* **1993**, *98*, 5648–5652.
- (52) Becke, A. D. *Phys. Rev. A* **1988**, *38*, 3098–3100.
- (53) Olsson, M. H. M.; Ryde, U. *J. Am. Chem. Soc.* **2001**, *123*, 7866–7876.
- (54) Pople, J. A.; Nesbet, R. K. *J. Chem. Phys.* **1954**, *22*, 571–572.
- (55) McWeeny, R.; Diercksen, G. *J. Chem. Phys.* **1969**, *49*, 4852–4856.
- (56) Wang, J. M.; Wang, W.; Kollman, P. A.; Case, D. A. *J. Mol. Graphics Modell.* **2006**, *25*, 247–260.
- (57) Case, D. A.; Darden, T. A.; Cheatham, T. E.; Simmerling, C. L.; Wang, J.; Duke, R. E.; Luo, R.; Merz, K. M.; Pearlman, D. A.; Crowley, M.; et al. *AMBER11*; University of California: San Francisco, CA, 2010.
- (58) Morris, G. M.; Goodsell, D. S.; Halliday, R. S.; Huey, R.; Hart, W. E.; Belew, R. K.; Olson, A. J. *J. Comput. Chem.* **1998**, *19*, 1639–1662.
- (59) Roothaan, C. C. *J. Rev. Mod. Phys.* **1951**, *23*, 69–89.
- (60) Yao, S.; Plastaras, J. P.; Marzilli, L. G. *Inorg. Chem.* **1994**, *33*, 6061–6077.
- (61) Cundari, T. R.; Fu, W.; Moody, E. W.; Slavin, L. L.; Snyder, L. A.; Sommerer, S. O.; Klinckman, T. R. *J. Phys. Chem.* **1996**, *100*, 18057–18064.
- (62) Lee, M. C.; Duan, Y. *Proteins* **2004**, *55*, 620–634.
- (63) Wang, J. M.; Wolf, R. M.; Caldwell, J. W.; Kollman, P. A.; Case, D. A. *J. Comput. Chem.* **2004**, *25*, 1157–1174.
- (64) Lavery, R.; Sklenar, H. *J. Biomol. Struct. Dyn.* **1988**, *6*, 63–91.
- (65) Lavery, R.; Moakher, M.; Maddocks, J. H.; Petkeviciute, D.; Zakrzewska, K. *Nucleic Acids Res.* **2009**, *37*, 5917–5929.
- (66) Srinivasan, J.; Cheatham, T. E.; Cieplak, P.; Kollman, P. A.; Case, D. A. *J. Am. Chem. Soc.* **1998**, *120*, 9401–9409.
- (67) Wang, W.; Lim, W. A.; Jakalian, A.; Wang, J.; Wang, J. M.; Luo, R.; Bayly, C. T.; Kollman, P. A. *J. Am. Chem. Soc.* **2001**, *123*, 3986–3994.

- (68) Yang, B.; Zhu, Y. Y.; Wang, Y.; Chen, G. J. *J. Comput. Chem.* **2011**, *32*, 416–428.
- (69) Kormos, B. L.; Benitex, Y.; Baranger, A. M.; Beveridge, D. L. *J. Mol. Biol.* **2007**, *371*, 1405–1419.
- (70) Jung, Y. W.; Lippard, S. J. *Chem. Rev.* **2007**, *107*, 1387–1407.
- (71) Temple, M. D.; McFadyen, W. D.; Holmes, R. J.; Denny, W. A.; Murray, V. *Biochemistry* **2000**, *39*, 5593–5599.
- (72) Kollman, P. A.; Massova, I.; Reyes, C.; Kuhn, B.; Huo, S.; Chong, L.; Lee, M.; Lee, T.; Duan, Y.; Wang, W.; et al. *Acc. Chem. Res.* **2000**, *33*, 889–897.
- (73) Pitié, M.; Pratviel, G. *Chem. Rev.* **2010**, *110*, 1018–1059.
- (74) Burrows, C. J.; Muller, J. G. *Chem. Rev.* **1998**, *98*, 1109–1152.
- (75) Liu, C. L.; Wang, M.; Zhang, T. L.; Sun, H. Z. *Coord. Chem. Rev.* **2004**, *248*, 147–168.
- (76) Balasubramanian, B.; Pogozelski, W. K.; Tullius, T. D. *Proc. Natl. Acad. Sci. U.S.A.* **1998**, *95*, 9738–9743.
- (77) Jin, Y.; Cowan, J. A. *J. Am. Chem. Soc.* **2005**, *127*, 8408–8415.
- (78) West, J. D.; Marnett, L. J. *Chem. Res. Toxicol.* **2006**, *19*, 173–194.
- (79) Chen, Z. F.; Wang, X. Y.; Li, Y. Z.; Guo, Z. J. *Inorg. Chem. Commun.* **2008**, *11*, 1392–1396.
- (80) Tu, C.; Shao, Y.; Gan, N.; Xu, D.; Guo, Z. J. *Inorg. Chem.* **2004**, *43*, 4761–4766.
- (81) Decker, A.; Chow, M. S.; Kemsley, J. N.; Lehnert, N.; Solomon, E. I. *J. Am. Chem. Soc.* **2006**, *128*, 4719–4733.
- (82) Neidle, S. *DNA Structure and Recognition*; Oxford University Press: Oxford, UK, 1994.
- (83) Pogozelski, W. K.; Tullius, T. D. *Chem. Rev.* **1998**, *98*, 1089–1108.